Röntgen materials for x-ray lasers-on-a-chip

Sharath Rameshbabu, Davide Bleiner

Sharath Rameshbabu, Davide Bleiner, "Röntgen materials for x-ray lasers-on-a-chip," Proc. SPIE 12582, Compact Radiation Sources from EUV to Gamma-rays: Development and Applications, 125820F (8 June 2023); doi: 10.1117/12.2665623

SPIE.

Event: SPIE Optics + Optoelectronics, 2023, Prague, Czech Republic

Röntgen Materials for X-Ray Lasers On-a-Chip

Sharath Rameshbabu[a,b], Davide Bleiner*[a,b]
[a]Swiss Federal Laboratories for Materials Science and Technologies, Überlandstrasse 129, 8600 Dübendorf, Switzerland; [b]Physics Institute, University of Zürich, Winterthurerstrasse 190, 8057, Zürich, Switzerland.

ABSTRACT

Compact X-Ray laser is a hot topic in the field of laser research, enabling 24/7 advanced spectroscopy and overcoming the beamline bottleneck. The investigated systems are either scaled-down replicas of accelerators, or tabletop architectures based on high-harmonic generation, plasmas, or wakefield acceleration. Ideally, one would enable a large range of applications if the X-Ray source would be portable. For that, some groups are working on accelerators-on-a-chip. A new class of active materials exploiting distributed feedback was proposed 50 years ago, as a candidate for an X-Ray laser gain medium. A Fabry-Perot analysis of a selection of "röntgen materials", based on their refractive index, Bragg's coupling coefficient, and threshold gain, is presented. The alkaline earth metal oxide showed the highest gain value of all the materials considered in this work. A relationship between the refractive index of the material and the threshold gain value is given. In addition, details on the geometry of the gain medium are discussed. Theoretical analysis revealed that alkaline earth metal oxides are a promising material with a higher gain coefficient of about 77.4 nm^{-1} for a 0.001 μm^3 crystal and the highest of all the materials investigated in this work. Except for alkaline earth metal oxide, all other oxide materials, such as transition and lanthanide metal oxide, have the lowest gain value. While nitrides, carbides, and compound semiconductors outperform oxide materials in terms of gain, they have still one order of magnitude less gain than alkaline earth metal oxide. The details of röntgen material calculations and design parameters are covered in depth.

Keywords: Röntgen material, X-Ray laser, compact, gain medium.

1. INTRODUCTION

The realization of X-Ray lasers as a tabletop setup is of great impact[1,2]. Presently, the shortest wavelength commercially available is at λ= 157 nm using a fluorine (F_2) excimer medium[3]. Cutting down the wavelength of two orders of magnitude to the X-Ray region is a hard task, due to the unfavorable wavelength-scaling between the spontaneous and stimulated emission, as predicted by the ratio of the Einstein coefficients A and B. Lasers with a wavelength down to the X-Ray region were demonstrated firstly by plasma-driven X-Ray sources, such as Ni-like Mo ions at 18.9 nm[4], Ag ions at 13.6 nm[5], Sn ions at 12 nm[6], Ba ions at 9.2 nm[7], Sm ions at 7.3 nm[8], Dy ions at 5.8 nm[9] and gold ions at 3.56 nm[10] based on transient collisional excitation[11]. Also recombination schemes were proposed, with high Stokes efficiency but difficult realization such as H-like C ions at 18.2 nm[12], Ne-like Ge ions at 19.6 nm[13], and few more. While great progress has been made[14,15], the greatest drawback with this technique is the requirement of a powerful external pump to create a high-energy plasma column[16], which operates in single pass without cavity.

Therefore, until now, synchrotron and free electron lasers are the most robust state-of-the-art for coherent X-Rays[17]. However, besides the difficulty to access the few worldwide beamlines, experiments must be ported to them. This poses a fundamental limitation for in situ environmental spectroscopy, industrial R&D, and biomedical application, to quote but a few. Several science cases require the tool to be portable in situ[18,19].

Having realized this, a few groups are working on the realization of an accelerator on a chip[20,21,22]. However, about 50 years ago, Fisher[23] proposed a concept to realize an X-Ray laser through distributed feedback in a single crystal. The main idea relies on the lattice plane of the crystal, which reflects the X-Ray as a Bragg mirror inside the gain medium, to accomplish distributed feedback (DFB). Indeed, if the X-Ray fluorescence wavelength is resonant with the crystal lattice (interplanar spacing), then there may be DFB of that particular wavelength through constructive feedback. This may lead to inversion and gain.

*davide.bleiner@empa.ch

Compact Radiation Sources from EUV to Gamma-rays: Development and Applications,
edited by Carmen S. Menoni, Jaroslav Nejdl, Proc. of SPIE Vol. 12582, 125820F
 · 0277-786X · doi: 10.1117/12.2665623

Fig. 1 summarizes the conceptual physics. Fluorescence that is resonant with the lattice characteristic lengthscales, can induce DFB and gain. Henceforth, the active medium is composed of the Bragg planes that make up the DFB nanocavity as well as the fluoresecence radiators. The detuning (lenght mismatch) between the fluorescence wavelength and lattice must be minimal. The radiators may be added through doping or from substrate pumping. A simple Fabry-Perot analysis is carried out here below. However, Yariv[24] has carried out detailed calculations for the practical X-Ray laser in waveguide-structured thin films. In particular, constraints on the values of the refractive indexes between the active medium and the cladding (substrate or superstrate) in which the active medium is embedded, were evaluated. These details will be the subject of future work regarding device integration. In fact, in DFB lasers, a corrugation (grating) is often introduced in one of the cladding layers. Here, this could derive from the high-frequency roughness of the substrate.

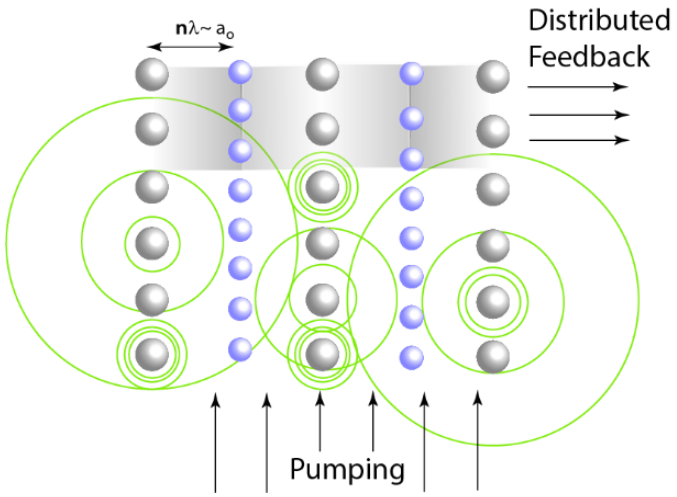

Fig. 1 Conceptual schematic of X-Ray laser working principle. Fluorescence that is resonant with the lattice lengthscale can induce distributed feedback and gain. See text for details.

The long-term aim of this work is to realize Fisher's concept laying here the foundation for an experimental device of a portable X-Ray laser on-a-chip. The materials are evaluated as a röntgen medium based on the following criteria:

1. d spacing of the selected material plane should fall within the X-Ray region,
2. Materials can be easily grown as a single crystalline,
3. Materials should be free from the crystal of hydration,
4. Chemically inert and
5. Vacuum compatible.

The various röntgen materials investigated for this work are summarized in Tables I–V. This paper is organized as follows: Section 2 explains a detailed theoretical investigation and requirements to meet the X-Ray laser through distributed feedback. Based on the discussion in Section 2, Tables I-V have been tabulated with various parameters such as Bragg's coupling coefficient, lasing gain, refractive index, etc; Section 3 briefs the characteristics of materials based on the fabrication and the chemical stability. A clear discussion on lasing gain and its dependency on the geometry of the gain medium was performed. Section 4 concludes the theoretical finding and possible outcome of this work.

2. Theory

Two conditions need to be met for lasing to happen: a phase resonance condition (**Eq. 1.a**) and the amplitude resonance condition (**Eq. 1.b**), summarized as follows:

$$\omega = m\pi c/(L\, n_e) \quad (1.a)$$

$$g_{mod} = (1/L)Ln(1/|r_1 r_2|) \quad (1.b)$$

with ω the angular frequency, m is an integer, L is the cavity length (in this simple Fabry-Perot analysis is the medium length-scale), n_e is the effective refractive index of the mode that travels through the structure, g_{mod} is the modal gain that

the wave experiences while traveling, a $r_{i=1,2}$ is the amplitude reflection coefficient of the absorber and spacer Bragg planes. The complete feedback system fulfills the condition for oscillation if:

$$r_1 r_2 Exp(g_{mod} L) Exp(-2i\beta L) = 1 \quad (2)$$

where the reflected wave travels back and it's again amplified (feedback) with a factor $Exp(g_{mod}L)$, while it gets a phase shift of $Exp(-2i\beta L)$. Note that the propagation constant $\beta = \frac{\omega n_e}{c}$ was used. Material gain and absorption are in the imaginary part of the complex refractive index. Therefore, the local complex refractive index was considered.
The gain medium must be a single crystal. Then, the d spacing has to be an integer multiple of the X-Ray wavelength, as given by the well-known Bragg equation,

$$2d\ sin\theta = n\lambda \quad (3)$$

where d is planar spacing, n is the order of reflection and λ is X-Ray wavelength. Two extreme cases are discussed, with intrinsic pumping and with external pumping, e.g. through the substrate. For instance, in SrO, the required resonant X-Ray fluorescence was generated from the Sr L_1-M_4 line (see **Table IV**), upon excitation. This was characterized as an intrinsic pumping mechanism as it was generated by the gain medium itself. Whereas, in Ho_2O_3, the required X-Ray fluorescence was generated from the Cu L_2-M_1 line (see **Table V**). Now, this will come under external pumping, as it will be generated from the substrate.
Let's consider only the cubic crystal in this work for simplicity and effectiveness. The structure factor (S) was calculated for the different crystal planes of the cubic crystal as follows:

$$S(hkl) = \sum_{i=1}^{N} f_i e^{2\pi i(hu_i + kv_i + lw_i)} \quad (4)$$

For instance, let's consider InP (fcc zinc blende structure). In InP, indium occupancy sites are (0,0,0), (0,1/2,1/2), (1/2,0,1/2), (1/2,1/2,0), and phosphorus occupancy sites are (3/4,1/4,1/4), (1/4, ¾, 1/4), (¼,1/4,3/4) and (3/4,3/4,3/4). Now plug in the values in **Eqn.4**, and we get S(100) = S(110) = 0 and S(111) = 4(f1+if2). As a further example, let's consider SrO (fcc NaCl structure). In SrO, strontium occupancy sites are (0,0,0), (0,1/2,1/2), (1/2,0,1/2), (1/2,1/2,0), and oxygen occupancy sites are (1/2,0,0), (0,1/2,0), (0,0,1/2) and (1/2,1/2,1/2). Following the same step as InP, S(100) = S(110) = 0 and S(111) = 4(f1+f2). From now on let's consider only (111) crystal plane in a cubic system for further calculation. The d-spacing corresponding to the (111) plane can be calculated as given below,

$$d_{111} = \frac{a_o}{\sqrt[2]{3}} \quad (5)$$

Where a_o is the lattice parameter Thus, equating **Eqn.3** and **Eqn.5**, one obtains a relationship that satisfies Bragg's condition as given below,

$$\frac{a_o}{\sqrt[2]{3}} = \frac{\lambda}{2} \quad (6)$$

Another critical parameter is Bragg's coupling coefficient (k) given by,

$$k = \frac{\omega\, n}{2c} \quad (7)$$

where ω is the X-Ray angular frequency, *n* is the refractive index of the medium and c is the speed of the light. The oscillation threshold gain is,

$$g = \left(\frac{1}{L^3}\right)\left(\frac{\pi}{k}\right)^2 \quad (8)$$

For one to realize a super-radiant or lasing action, gL ≥ 1, where L is the length of the gain medium.

Let's consider one particular case as CaO, a_0 = 4.81 Å, d_{111} = 2.78 Å, n = 0.632x10^{-4} (obtained from the CXRO database). Using **Eqn.7**, k was found as 3571 cm^{-1}. Substituting all these values into **Eqn.8**, the gain was calculated as 77.4 nm^{-1} for 0.001 μm^3 volume of the gain medium. In this case, gL = 7740 (gain medium length = 100 nm, LxBxH = 100nm x 100nm x 100nm). If we consider the larger crystal size of 1 μm^3 (LxBxH = 1μm x 1μm x 1μm) then, gL = 77.4, and increasing the crystal size to 10^6 μm^3 (LxBxH = 100μm x 100μm x 100μm) then, gL = 0.0774. These results indicate that crystals less than 100 μm would be required, which is promising for micro-integration on-a-chip. Next comes the experimental challenge for the fabrication of such a small device. So we proposed the possibility of the pulsed laser deposition for the epitaxial thin film growth, and later using the lithography technology, we could pattern the required crystal dimension by etching.

Table I. Group II-VI, III-V, IV semiconductor material (1- from the NIST database, 2- from the CXRO database. The lattice parameter was obtained from the materials project)

Material#	**Lattice parameter (Å)**	**Resonant line[1]**	**Resonant Fluorescence wavelength[1] (Å)**	**Relative detuning (%)**	**Refractive index[2] at wavelength (×10^{-4})**	**Bragg's coupling coefficient (×$10^3$$cm^{-1}$)**	**Lasing gain (nm^{-1})**
CdTe	6.48	Sr L_3-M_2	7.46	-0.27	3.259	13.699	5.26
InSb	6.48	Sr L_3-M_2	7.46	-0.27	3.295	13.850	5.15
PbTe	6.46	Sr L_3-M_2	7.46	0.00	5.284	22.210	2.00
GaSb	6.10	Rb L_2-M_5	7.07	0.42	3.241	14.385	4.77
InAs	6.06	Y L_3-M_3	6.96	-0.57	3.680	16.581	3.59
CdSe	6.05	Y L_3-M_3	6.96	-0.43	4.183	18.848	2.78
PbS	5.94	Sr L_3-M_4	6.87	0.15	4.302	19.654	2.56
InP	5.87	Rb L_2-N_1	6.77	-0.15	3.523	16.326	3.70
CdS	5.83	Y L_2-M_2	6.73	0.00	2.326	10.855	8.38
AlAs	5.66	Zr L_3-M_3	6.55	0.15	1.834	8.785	12.79
Ge	5.66	Zr L_3-M_3	6.55	0.15	2.576	12.339	6.48
GaAs	5.65	Nb L_3-M_1	6.52	0.00	2.538	12.225	6.60
AlP	5.45	Sr L_2-N_1	6.29	0.00	1.102	5.496	32.67
GaP	5.45	Sr L_2-N_1	6.29	0.00	1.564	9.330	11.34
Si	5.43	Nb L_3-M_2	6.22	-0.80	1.039	5.240	35.95
ZnS	5.42	Zr L_2-M_3	6.27	0.16	1.946	10.050	9.77

Table II. 3-d transition metal nitride (1- from the NIST database, 2- from the CXRO database. The lattice parameter was obtained from the materials project)

Material#	**Lattice parameter (Å)**	**Resonant line[1]**	**Resonant Fluorescence wavelength[1] (Å)**	**Relative detuning (%)**	**Refractive index[2] at wavelength (×10^{-4})**	**Bragg's coupling coefficient (×$10^3$$cm^{-1}$)**	**Lasing gain (nm^{-1})**
ScN	4.51	Ru L_3-M_3	5.21	0.00	1.025	6.168	25.94
TiN	4.24	Tc L_2-M_4	4.89	-0.15	1.551	9.956	9.96
VN	4.12	Pd L_3-M_2	4.74	-0.42	1.698	11.233	7.82
CrN	4.19	Mo L_2-N_1	4.83	-0.21	2.124	13.802	5.18
MnN	4.14	Tc L_1-M_2	4.78	0.00	2.084	13.690	5.27
FeN	4.20	Mo L_2-N_1	4.83	-0.41	2.383	15.284	4.23
CoN	4.22	Zr L_1 edge	4.88	0.21	2.697	17.345	3.28

Table III. 3-d transition metal carbide and oxide (1- from the NIST database, 2- from the CXRO database. The lattice parameter was obtained from the materials project)

Material[#]	**Lattice parameter (Å)**	**Resonant line[1]**	**Resonant Fluorescence wavelength[1] (Å)**	**Relative detuning (%)**	**Refractive index[2] at wavelength ($\times 10^{-4}$)**	**Bragg's coupling coefficient ($\times 10^3 cm^{-1}$)**	**Lasing gain (nm^{-1})**
Sc_4C_3(110)	7.21	Ge L_2-M_4	10.17	-0.30	3.951	12.188	6.64
Ti_2C	8.62	Se L_2-M_1	9.95	0.00	5.603	17.670	3.16
Sc_2O_3(110)	9.86	Ni L_2 edge	13.97	0.14	7.343	16.486	3.63
V_2O_3 (110)	9.57	Co L_1-M_4	13.41	-0.97	13.294	31.098	1.02
NiO	4.19	Mo L_2-N_1	4.83	-0.21	2.047	13.294	5.59
Cu_2O	4.25	Mo L_3-N_4	4.92	0.20	2.717	17.339	3.28

Table IV. Alkaline earth metal oxide (1- from the NIST database, 2- from the CXRO database. The lattice parameter was obtained from the materials project)

Material[#]	**Lattice parameter (Å)**	**Resonant line[1]**	**Resonant Fluorescence wavelength[1] (Å)**	**Relative detuning (%)**	**Refractive index at wavelength[2] ($\times 10^{-4}$)**	**Bragg's coupling coefficient ($\times 10^3 cm^{-1}$)**	**Lasing gain (nm^{-1})**
MgO	4.21	Ru L_2-M_3	4.95	1.81	1.200	7.613	17.03
CaO	4.81	Tc L_3-M_2	5.56	0.18	0.632	3.571	77.40
SrO	5.17	Sr L_1-M_4	5.96	-0.17	0.810	4.263	54.31
BaO	5.58	Y L_3-M_5	6.45	0.16	1.478	7.194	19.07

Table V. Lanthanide metal oxide, carbide and nitride (1- from the NIST database, 2- from the CXRO database. The lattice parameter was obtained from the materials project)

Material[#]	**Lattice parameter (Å)**	**Resonant line[1]**	**Resonant Fluorescence wavelength[1] (Å)**	**Relative detuning (%)**	**Refractive index[2] at wavelength ($\times 10^{-4}$)**	**Bragg's coupling coefficient ($\times 10^3 cm^{-1}$)**	**Lasing gain (nm^{-1})**
La_2O_3(110)	11.36	Mn L_1-N_1	15.99	-0.50	7.467	14.650	4.60
Gd_2O_3(110)	10.81	Cu L_3-M_1	15.29	0.00	11.702	24.038	1.71
Ho_2O_3(110)	10.52	Cu L_2-M_1	14.88	0.00	13.364	28.121	1.25
Lu_2O_3(110)	10.26	Ni L_3-M_5	14.51	0.00	15.183	32.809	0.92
La_2C_3(110)	8.83	Na K-L_1	12.49	0.00	6.257	15.914	3.89
Gd_2C_3(110)	8.34	Zn L_2 edge	11.80	0.00	5.780	15.914	4.17
Ho_2C_3(110)	8.16	Na K-M_1	11.54	0.00	7.467	20.277	2.40
Lu_2C_3(110)	8.01	Cu L_1-N_1	11.30	-0.27	9.126	25.299	1.54
LaN	5.30	Rb L_1-N_1	6.10	-0.33	2.345	12.057	6.79
GdN	4.98	Y L_2-N_4	5.75	0.00	2.579	14.085	4.98
HoN	4.86	Y L_1-M_4	5.61	0.00	2.350	13.156	5.70
LuN	4.72	Zr L_2-N_2	5.45	0.00	2.339	13.473	5.44

All the materials considered with (111) plane unless otherwise specified.

Relative detuning is the mismatch between the inter-planar distance and the resonant pump line. It is calculated as follows, $(\lambda - d)/_{\lambda}$ For example: in LuN, λ = 5.45Å, d = 5.45Å, detuning is 0.00%

3. RESULTS AND DISCUSSION

This study analyzed a variety of röntgen materials, such as alkaline metal oxides, compound semiconductors, 3-d transition metal oxides, nitride, carbides, and lanthanides. The materials are grouped based on their unit cell length in **Fig.2** because the lattice parameter determines the d-spacing, which is directly proportional to the resonant X-Ray wavelength. The graph shows a general trend in which the lasing gain increases as the resonant X-Ray wavelength decreases, which was attributed to the material's refractive index. Nitrides have the lowest refractive index, as low as 1.025 x 10^{-3} for ScN, as compared to oxides and carbides, and a decrease in a refractive index reduces Bragg's coupling coefficient, as given by **Eqn.7**. As shown in **Eqn.8**, a lower Bragg's coupling co-efficient increases the threshold gain, which is inversely proportional to the square of the Bragg's coupling co-efficient. As an example, alkaline metal oxide has the highest gain value due to the material's extremely low refractive index values (almost an order less than nitrides).

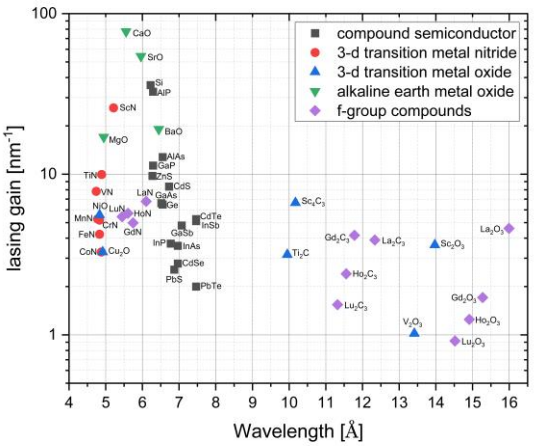

Fig. 2 Lasing gain as a function of resonant X-Ray wavelength for various röntgen materials. See text for details.

Fig.2 summarizes a large selection of compounds in terms of optical behavior (i.e. gain), whereas CaO and SrO are superior among any considered material. To satisfy the distributed feedback, the materials used as the gain medium should be the source of the resonant X-ray. In such conditions, the emitted radiation can reinforce the pumping field with secondary or tertiary fluorescence of lattice atoms. This only occurs in SrO, where the Sr L1M4 line matches the lattice spacing with -0.17 % relative detuning. Therefore, SrO is the best candidate with the relatively highest gain and meeting distributed feedback conditions.

According to **Eqn.8**, the lasing gain is inversely proportional to the volume of the gain medium, which in our instance can be discretized into cross-section area (a,b nm) and gain medium length (c nm). To improve the gain value, volume can be reduced by reducing the cross-section area or the length of the gain medium, or both. For the lasing action and increased saturation, the length of the gain medium must be greater than the other two dimensions of the gain medium (area). Gain-saturation can be calculated using the formula given by **Eqn.9** for cubic geometry[25],

$$G_{sat} = 2.53 + 2ln\left(\frac{Z}{X}\right) \quad (9)$$

where Z is the length of the gain medium and X and Y are the sides of the gain medium. If all the dimensions of the gain medium are equal, then G_{sat} = 2.53. To increase the gain saturation one needs to increase the length of the gain medium along with the reduction of the volume. For example, (z/x) = 10, then G_{sat} = 7.14.
Keeping the same area and increasing the length of the gain medium drops the gain value as the volume increases. At the same time, the length of the gain medium cannot be reduced more than the other two dimensions of the gain medium. For example if (z/x) = 0.1, then G_{sat} = -2.08. Here the negative sign indicates absorption rather than emission. The better way to get an increase in the gain value is to reduce the cross-sectional area rather than the length of the gain medium. Thus, the gain length product will scales up with the length of the gain medium.

3.1 MATERIALS CHARACTERISTICS

To obtain an epitaxial thin film with stoichiometry control, we can opt for PLD, MBE (molecular beam epitaxy), or ALD (atomic layer deposition). PLD is suitable to grow most of the material considered for this study and it is well known for stoichiometric thin film growth. Nitride film is a challenging material to grow by PLD or any mentioned technique due to the stability of nitrogen molecules. For nitride and oxide thin film growth, background reactive nitrogen and oxygen environments were required to form nitride and oxide films, respectively. Thus, major challenges in obtaining epitaxial thin film by PLD require optimization of background pressure, substrate temperature, and repetition rate of pulsed laser used for ablation.

The most important consideration of the gain medium is its chemical stability. The material should have a high melting point, good electrical conductivity, and be chemically inert. As discussed above, SrO is highly unstable in the presence of moisture and CO_2. Generally, all earth metal oxides tend to hydrolyze in the presence of moisture and convert to carbonates by absorbing CO_2 from the environment. Most of the oxides, particularly lanthanide oxides, are wide bandgap semiconductors. If we use electrons to pump our active medium, then they could have a charging effect due to the insulating property. However, lanthanide oxides have a higher melting point, above 2500^{o}C. On the other hand, nitrides are metallic, but as discussed, they are difficult to fabricate in stoichiometry. In terms of chemical stability, transition metal nitrides are chemically inert, but lanthanide nitrides are unstable in a humid environment.

4. CONCLUSION

A Fabry-Perot calculation for the X-Ray laser using single crystal röntgen material at various wavelengths was carried out. Since X-Ray reflectivity depends on the lattice plane, the wavelength of the laser becomes dependent on the material property. In general, materials with small unit cells have the lowest output wavelength. The gain of the laser with different materials was calculated and tabulated and it concludes the gain dependency on the refractive index of the material. Materials with the lowest refractive index such as CaO and SrO have the highest gain value of the considered materials. Various optical, chemical, fabrication, and commercial characteristics of materials were discussed and lanthanide oxide was found to be a good candidate for a gain medium. Then, the lasing gain value dependency on the dimension of the gain medium was compared for different dimensions of SrO material. The gain value is increasing with a reduction of the gain medium volume. The gain saturation value is comparable to obtaining a net gain when the length of the gain medium is at least equal to the other two dimensions. In the present study, 0.001 μm^3 crystal was considered and for all the materials, the gain-length product is much larger than the gain saturation. From the optical characteristics, SrO looks like a good candidate, but it has lots of challenges, such as poor chemical stability. Thus, primarily looking into the material's stability lanthanide oxides are better in terms of fabrication, have higher melting points, and are chemically inert with only the disadvantage of wide bandgap semiconductor. We can overcome this disadvantage by neglecting the electron beam as our pumping mechanism. In terms of commercial value, rare earth is quite expensive compared with other elements. As mentioned above about the need for a metal-organic precursor for the atomic layer deposition (ALD) technique, they are expensive, toxic, corrosive, and flammable. In terms of material usage and cost, pulsed laser deposition (PLD) will be the best option to be used for thin film deposition, as it required less material.
The analytical consideration for the X-Ray laser is promising but the greater practical challenge is associated with the realization of such small single crystals, matching along with the resonant X-Ray wavelength source.

ACKNOWLEDGEMENT

This work was supported by the Swiss National Science Foundation (SNSF) under grant number 204442.

REFERENCES

[1] Bleiner, Davide. "The science and technology of X-ray lasers: a 2020 update." In International Conference on X-Ray Lasers 2020, vol. 11886, p. 1188602. SPIE, (2021).

[2] Balmer, Juerg E., Davide Bleiner, and Felix Staub. "Extreme ultraviolet lasers: principles and potential for next-generation lithography." Journal of Micro/Nanolithography, MEMS, and MOEMS 11, no. 2, 021119-021119 (2012).

[3] Craighead, Harold G., J. C. White, R. E. Howard, L. D. Jackel, R. E. Behringer, J. E. Sweeney, and R. W. Epworth. "Contact lithography at 157 nm with an F2 excimer laser." Journal of Vacuum Science & Technology B: Microelectronics Processing and Phenomena 1, no. 4, 1186-1189 (1983).

[4] Booth, N., M. H. Edwards, Z. Zhai, G. J. Tallents, T. Dzelzainis, C. L. S. Lewis, A. Behjat et al. "Grazing incidence pumping of an 18.9 nm Ni-like Mo X-ray laser." The European Physical Journal Special Topics 175, 153-158 (2009).

[5] Wang, Yet al, M. A. Larotonda, B. M. Luther, D. Alessi, M. Berrill, V. N. Shlyaptsev, and J. J. Rocca. "Demonstration of high-repetition-rate tabletop soft-X-Ray lasers with saturated output at wavelengths down to 13.9 nm and gain down to 10.9 nm." Physical Review A 72, no. 5, 053807 (2005).

[6] Yan, Fei, Jie Zhang, Xin Lu, and Jia Y. Zhong. "Design of the nickel-like tin X-Ray laser at 12.0 nm." JOSA B 22, no. 4, 786-791 (2005).

[7] Staub, Felix, C. Imesch, Davide Bleiner, and J. E. Balmer. "Soft-X-ray lasing in nickel-like barium at 9.2 nm using the grazing-incidence scheme." Optics communications 285, no. 8, 2118-2121 (2012).

[8] Lin, J. Y., G. J. Tallents, R. Smith, A. G. MacPhee, E. Wolfrum, J. Zhang, G. Eker et al. "Optimization of double pulse pumping for Ni-like Sm X-Ray lasers." Journal of applied physics 85, no. 2 (1999): 672-675.

[9] Rockwood, Alex, Yong Wang, Shoujun Wang, Mark Berrill, Vyacheslav N. Shlyaptsev, and Jorge J. Rocca. "Compact gain-saturated X-Ray lasers down to 6.85 nm and amplification down to 5.85 nm." Optica 5, no. 3, 257-262 (2018).

[10] Nickles, P. V., K. A. Janulewicz, and W. Sandner. "Table-Top X-Ray Lasers in Short Laser Pulse and Discharge Driven Plasmas." Strong Field Laser Physics, 321-378 (2009).

[11] Balmer, J. E., Felix Staub, Christoph Imesch, and D. Bleiner. "Sub-10-nm wavelength Ni-like-ion collisional x-ray lasers." In X-ray Lasers and Coherent X-ray Sources: Development and Applications IX, vol. 8140, pp. 199-203. SPIE, (2011).

[12] Lee, K., and D. Kim. "Another regime of operation for a 18.2 nm recombination laser using a capillary-discharged carbon plasma." Applied Physics Letters 79, no. 13, 1968-1970 (2001).

[13] Nantel, M., J. C. Kieffer, B. La Fontaine, H. Pépin, G. D. Enright, D. M. Villeneuve, J. Dunn, H. A. Baldis, and O. Peyrusse. "Dynamics of Ne-like populations in the germanium x-ray laser." Physics of Fluids B: Plasma Physics 5, no. 12, 4465-4472 (1993).

[14] Ruiz-Lopez, Mabel, and Davide Bleiner. "Implementing the plasma-lasing potential for tabletop nano-imaging." Applied Physics B 115, 311-324 (2014).

[15] Masoudnia, Leili, Mabel Ruiz-Lopez, and Davide Bleiner. "Table-top two-color soft X-ray laser by means of Ni-like plasmas." Physics of Plasmas 23, no. 4, 043108 (2016).

[16] Bleiner, Davide, Jürg E. Balmer, and Felix Staub. "Line focusing for soft x-ray laser-plasma lasing." Applied optics 50, no. 36, 6689-6696 (2011).

[17] Ruiz-Lopez, Mabel, A. Faenov, T. Pikuz, N. Ozaki, A. Mitrofanov, B. Albertazzi, N. Hartley et al. "Coherent X-ray beam metrology using 2D high-resolution Fresnel-diffraction analysis." Journal of synchrotron radiation 24, no. 1, 196-204 (2017).

[18] Müller, Rafael, Ilya Kuznetsov, Yunieski Arbelo, Matthias Trottmann, Carmen S. Menoni, Jorge J. Rocca, Greta R. Patzke, and Davide Bleiner. "Depth-profiling microanalysis of CoNCN water-oxidation catalyst using a λ= 46.9 nm plasma laser for nano-ionization mass spectrometry." Analytical chemistry 90, no. 15 (2018): 9234-9240.

[19] Bleiner, Davide, Felix Staub, Vitaliy Guzenko, Yasin Ekinci, and Jürg E. Balmer. "Evaluation of lab-scale EUV microscopy using a table-top laser source." Optics communications 284, no. 19 (2011): 4577-4583.

[20] Hakimi, Sahel, Xiaomei Zhang, Calvin Lau, Peter Taborek, Franklin Dollar, and Toshiki Tajima. "X-ray laser wakefield acceleration in a nanotube." International Journal of Modern Physics A 34, no. 34, 1943011 (2019).

[21] England, R. Joel, Peter Hommelhoff, and Robert L. Byer. "Microchip accelerators." Physics Today 74, no. 8 (2021).

[22] Assmann, R. W., M. K. Weikum, T. Akhter, D. Alesini, A. S. Alexandrova, M. P. Anania, N. E. Andreev et al. "EuPRAXIA conceptual design report." The European Physical Journal Special Topics 229, no. 24, 3675-4284 (2020).

[23] Fisher, Robert A. "Possibility of a distributed-feedback x-ray laser." Applied Physics Letters 24, no. 12, 598-599 (1974).

[24] Yariv, Amnon. "Analytical considerations of Bragg coupling coefficients and distributed-feedback x-ray lasers in single crystals." Applied Physics Letters 25, no. 2, 105-107 (1974).

[25] Bleiner, Davide. "Saturation gain-length product during short-wavelength plasma lasing." Applied physics letters 101, no. 8, 081105 (2012).